Theor Chem Acc (2012) 131:1146
DOI 10.1007/s00214-012-1146-6

REGULAR ARTICLE

Achieving fast convergence of ab initio free energy perturbation calculations with the adaptive force-matching method

Eric R. Pinnick · Camilo E. Calderon · Andrew J. Rusnak · Feng Wang

Received: 19 June 2011 / Accepted: 9 September 2011 / Published online: 19 February 2012

Abstract This paper studies the possibility of improving the convergence of ab initio free energy perturbation (FEP) calculations by developing customized force fields with the adaptive force-matching (AFM) method. The ab initio FEP method relies on a molecular mechanics (MM) potential to sample configuration space. If the Boltzmann weight of the MM sampling is close to that of the ab initio method, the efficiency of ab initio FEP will be optimal. The difference in the Boltzmann weights can be quantified by the relative energy difference distribution (REDD). The force field developed through AFM significantly improves the REDD when compared with standard MM models, thus improving the convergence of the ab initio FEP calculation. The static dielectric constant ε_s of ice-Ih was studied with PW-91 through ab initio FEP. With a customized force field developed through AFM, we were able to converge ε_s to 80 ± 4 with 3,600 configurations. A similar ab initio FEP calculation with the TIP4P model would require 220 times more configurations to achieve the same accuracy. Our study indicates that the PW-91 functional underestimates ice-Ih ε_s by about 20%.

Keywords Ab initio free energy perturbation · Adaptive force-matching · Static dielectric constant · Ice

Published as part of the special collection of articles: From quantum mechanics to force fields: new methodologies for the classical simulation of complex systems.

E. R. Pinnick · C. E. Calderon · A. J. Rusnak · F. Wang (✉)
Boston University, Boston, MA, USA
e-mail: fengwang@bu.edu

1 Introduction

In a sense, accurate determination of potential energy surfaces (PESs) of molecular systems can be considered a solved problem. With a sufficiently high level of correlation and a large enough basis set, post-Hartree–Fock (post-HF) methods such as many-body perturbation theory [1–5], configuration interaction [6–8], and coupled cluster (CC) [9, 10] can, in principle, provide arbitrarily high accuracy within the Born-Oppenheimer approximation. In practice, however, most post-HF methods scale as high-order polynomials of system size, and accurate PES determination quickly becomes computationally intractable.

Recent advances in computational chemistry have gone a long way toward reducing the computational cost of post-HF methods. For example, variants of the MP2 method [2, 4, 11] such as RI-MP2 [12, 13] and LMP2 [14–16] have been made so efficient that systems with a few hundred atoms can be described with reasonable computational cost. However, for even larger systems or for systems that require higher order treatment of correlation, one would have to resort to density functional theory (DFT).

DFT provides a good trade-off between cost and accuracy [17–19]. Relying on a mean field approximation similar to Hartree–Fock, DFT produces surprisingly high accuracy for a wide range of problems and has become the de facto standard to obtain PESs for systems that are computationally intractable with more rigorous post-HF treatments. Due to the simplicity of the DFT formalism, near-linear scaling computational cost is a real possibility [20–25]. The popular Kohn-Sham DFT implementations can model systems with around one thousand atoms; methods such as orbital-free DFT [17, 26–29] and other variants have been applied to even larger systems.

In addition, DFT has been used to drive molecular dynamics sampling, although the time scale that can be achieved by DFT-based molecular dynamics is typically limited to tens of picoseconds. Sampling any non-trivial configuration space at nano-second time scale or longer with an electronic-structure method is likely to remain a significant challenge for years to come.

In this paper, we explore the possibility of using the recently proposed adaptive force-matching (AFM) method to parameterize a customized potential to best reproduce the PES of an electronic-structure method [30–34]. The AFM potential will be used to perform sampling on the electronic-structure-quality PES. This approach significantly extends the time scale that can be sampled with electronic-structure PES. The configurations sampled with the AFM force field will be used to calculate ensemble properties using the ab initio free energy perturbation (FEP) approach [35–38]. We demonstrate that such an approach is much more efficient than performing ab initio FEP with a non-customized molecular mechanics (MM) potential.

Philosophically, our AFM method bears some resemblance to the work by Ischtwan and Collins [39], where a potential energy surface sampled from a MM potential is successively improved by additional electronic-structure calculations. However, the Collins approach never reparametrizes the MM potential used for sampling.

In Sect. 2, we provide a brief introduction of the AFM method; in Sect. 3, we briefly review the ab initio FEP method; in Sect. 4, we demonstrate the use of an AFM force fields with ab initio FEP to calculate the static dielectric constant of ice-Ih; a summary will be provided in Sect. 5.

2 The adaptive force-matching method

The AFM method is designed to parameterize an otherwise general-purpose force field to a set of thermodynamic conditions related to the investigation of one specific problem. A typical MM force field is composed of rather simple energy expressions. These force fields are often required to be transferable so that they can model a range of molecules under different thermodynamic conditions. Due to the simplicity of the energy expressions, requiring a force field to be transferable will lead to compromises in accuracy. When the force field parameters are required to be balanced for all conditions, they cannot provide optimal accuracy for any one condition.

Because molecular interactions are dictated by complicated quantum mechanical forces between the electrons and between the electrons and nuclei, modeling these quantum interactions accurately with a transferable potential is extremely challenging. In the context of force field development, these quantum interactions are typically classified into more intuitive physical concepts. A very short and incomplete list includes the various types of molecular orbital interactions, polarization, dispersion, charge transfer, exchange-repulsion, and charge penetration [40–50]. Capturing all these quantum mechanical interactions through MM is a grand challenge that is extremely difficult to solve. It is likely that once all quantum mechanical interactions are represented appropriately, a truly transferable and accurate MM force field may be as computationally demanding as an electronic-structure method.

Fortunately, modeling any one specific problem requires only a small variety of molecules to be simulated under a limited number of thermodynamic states. The philosophy of AFM is to generate problem-specific force fields. AFM is designed to adapt an otherwise general-purpose force field to answer one specific question with the best possible accuracy. Within the limitation of simple force field expressions, AFM achieves better accuracy by sacrificing transferability. For example, if the melting temperature of ice-Ih is to be determined, the AFM force field will be required to describe water interactions around the melting point in both the liquid and the solid phases. Being able to describe water interactions in a hydrophobic environment or at higher temperatures is irrelevant for ice melting and therefore not necessary for that force field to model.

When designing a problem-specific force field, the answer to the question being addressed should not be fitted. In fact, no experimental properties are fitted in the AFM approach. Our published works only fit atomic forces and molecular forces and torques from electronic-structure calculations. AFM uses an iterative mechanism to create a training set that is most representative of the target configuration space. AFM also provides a mechanism to adjust the cost of the electronic-structure calculations allowing the least expensive electronic-structure method for a desired accuracy to be used [30]. Previous realizations of AFM utilize the singular value decomposition (SVD) method to obtain parameters [51, 52]. SVD guarantees the global minimum of the objective function to be identified but is restricted to the use of linear parameters in the force field. Fortunately, most standard force field terms can be fit using just linear parameters.

Starting from an initial guess force field, a typical AFM study is composed of three steps:

The sampling step: In the sampling step, the guess force field is used to sample the configuration space most relevant to the question under investigation. If the configuration space is difficult to transverse, an enhanced sampling method can be applied to ensure proper sampling of all important basins in free energy. If the force field is

expected to model several state points, an independent sampling can be performed for each state point. Configurations from all the state points will be fed to the next step.

The ab initio step: Taking configurations from the sampling step, quantum mechanics (QM) or QM/MM calculations will be performed to obtain reference forces for subsequent fitting. Published work from our group has mostly focused on using QM/MM methods in the ab initio step [30–32, 34]. The use of QM/MM allows post-HF methods to be used for the QM region. The accuracy of the QM forces can be judged by performing convergence tests with regard to the size of the QM region, the level of theory, and the basis set [31]. Convergence tests can provide information for minimizing the computational cost of QM/MM calculations while maintaining the desired accuracy. The maximum accuracy achievable by the force field can be established by calculating the root mean square error (RMSE) of the fit in the fitting step. Since the maximum accuracy is frequently bottlenecked by the quality of the energy expressions, performing QM/MM calculations with a quality much higher than that provided by the energy expressions is not necessary.

The fitting step: After QM forces are obtained, the force field will be parameterized to best reproduce the QM forces. This can be accomplished with a two-step process by minimizing the molecular force RMSE,

$$\chi^2_{\text{mole}} = \sum_i w_i \left(F_i^{\text{ref}} - F_i^{\text{fit}}\right)^2 + \sum_i u_i \left(\tau_i^{\text{ref}} - \tau_i^{\text{fit}}\right)^2 + \lambda \sum_\mu \left(\sum_v n_v q_{\mu v} \right), \quad (1)$$

in the first step and the atomic force RMSE,

$$\chi^2_{\text{atom}} = \sum_m s_m \left[f^{\text{fit}}_{\text{intra},m} + f^{\text{fit}}_{\text{mole},m} - f_i^{\text{ref}} \right]^2, \quad (2)$$

in the second step.

In the first step, only intermolecular parameters are being determined. In the last term of Eq. 1, q_{uv} is the product of charges on atoms u and v; this term is included to ensure charge neutrality when SVD is used to fit Eq. 1 [31, 53]. Since SVD can only fit linear parameters, only products of charges can be fit. The partial charges are solved using a system of nonlinear equations from the knowledge of charge products. w_i and u_i in Eq. 1 are relative weights, and we typically use

$$w_i = \frac{s_i}{\sum_i s_i |F_i^{\text{ref}}|^2}, \quad (3)$$

and

$$u_i = \frac{s_i}{\sum_i s_i |\tau_i^{\text{ref}}|^2}, \quad (4)$$

where s_i is the solvation parameter chosen to be one for molecules buried in the QM region and zero for molecules at the interface [32]. The solvation parameters are used to remove QM/MM interface molecules from the fit; the forces on QM molecules at interface are influenced by the presence of nearby MM particles and are not a good reflection of the true QM PES. The sum of square forces and square torques is used in Eqs. 3 and 4 to make the molecular force and torque terms in Eq. 1 dimensionless.

In the second step, the intramolecular parameters are optimized to make the sum of the intramolecular forces, $f^{\text{fit}}_{\text{intra},m}$, and the intermolecular forces, $f^{\text{fit}}_{\text{mole},m}$, best reproduce the reference QM forces f_i^{ref}. $f^{\text{fit}}_{\text{mole},m}$ is calculated using the intermolecular parameters obtained in the first step, and s_{m} is the solvation parameter.

We prefer a two-step fitting procedure, because it is more important for a force field to provide a good description of intermolecular interactions when compared with intramolecular interactions. A two-step fitting procedure should not be considered to be set in stone. One could imagine all parameters to be fit in one step with appropriate weights applied to intermolecular and intramolecular terms. For protein molecules, one could consider fitting inter-residue forces and intra-residue forces separately.

If possible, we prefer to use the SVD method to fit the force field parameters. As mentioned previously, the SVD method guarantees the global minimum of the objective function to be obtained. On the other hand, SVD requires the forces to be linear functions of the parameters. To date, we have been able to fit harmonic, quartic, and Morse bond terms, harmonic and quartic angle terms, harmonic cosine dihedral terms, Lennard-Jones interactions, and a hydrogen-bond terms with SVD [30–34]. The only term we fit nonlinearly is the exponential parameter in a Buckingham potential.

After the fitting step, the forces produced by the new force field will better represent the QM forces. With the improved accuracy, the new force field will lead to better sampling and will improve the quality of the QM/MM calculations in the ab initio step. When QM/MM calculations are performed in the ab initio step, the improved MM parameters will provide a better representation of the true electrostatic environment for the QM region through Coulombic embedding.

Each iteration of these three steps will be referred to as a generation of AFM. Several generations of AFM will be performed until convergence is reached. Typically, additional generations are run even after convergence to allow all the QM forces from all the converged generations to be fit together in a global fit. The objective of the global fit is to reduce the error bar on the final parameters.

3 Ab initio free energy perturbation method

The free energy perturbation (FEP) method was introduced by Zwanzig [54] in 1954. Assuming an ensemble of configurations governed by a Hamiltonian H_1 is sampled, the FEP approach allows thermodynamic properties of a different ensemble governed by Hamiltonian H_2 to be determined by reweighing the configurations sampled with H_1. Although the FEP approach is most frequently used to calculate the free energy of a different Hamiltonian [55, 56], as outlined in the original Zwanzig paper, it is applicable to any thermodynamic property that can be determined from the partition function. One popular application of FEP is the ab initio FEP approach [35–38]. In ab initio FEP, the H_1 for sampling is an MM force field. Thermodynamic properties associated with an electronic-structure Hamiltonian H_2 can be calculated by reweighting each configuration in the MM partition function by $\exp[(U_F - U_A)/k_BT]$, where U_A is the configuration energy according to the electronic-structure method and U_F is the configuration energy of the force field [57].

Due to the exponential factor in the weight, FEP will not converge with any practical sample size unless the difference between the two Hamiltonians is sufficiently small. The difference between the two Hamiltonians can be judged by studying the distribution of $U_F - U_A$. When the MM force field exactly reproduces the QM PES, the distribution of $U_F - U_A$ will be a δ function. Thus, all the exponential weights will be identical to $\exp[(\Delta U_0)/k_BT]$, where ΔU_0 is the difference between the zeros of energies for the MM and electronic-structure PES. It can be easily shown that for the calculation of any property using ab initio FEP, the result does not depend on ΔU_0. When the distribution of $U_F - U_A$ is calculated, we choose the medians of the distributions of both the QM and MM energies to be zero, thus making $\Delta U_0 = 0$. We will refer to the distribution of $U_F - U_A$ as the FEP relative energy difference distribution (REDD) in the subsequent discussions.

When ab initio FEP is applied, an off-the-shelf MM force field is frequently used without checking the REDD. In this work, we propose to use AFM to fit an MM potential to ab initio forces. We demonstrate that the force field fit by AFM provides a much better description of the QM PES. The standard deviation of the REDD is much narrower when an AFM force field is used when compared with off-the-shelf potentials. The significantly narrower distribution allows FEP to converge exponentially faster. In addition, other methods designed to reduce the error of ab initio FEP can be used together with a customized AFM force field [58].

4 Calculation of the static dielectric constant of ice-Ih with ab initio FEP and AFM

In order to demonstrate the effectiveness of combining an AFM force field with ab initio FEP, we decided to calculate the static dielectric constant ε_s of ice-Ih. The calculation of ε_s for ice is notoriously challenging even with an MM potential [59–63]. Although the dielectric constant associated with electronic polarization in ice-Ih has been determined using DFT [64], to the best of our knowledge, ε_s for ice-Ih has not been calculated with an electronic-structure method.

The ε_s for ice-Ih is larger than the ε_s of liquid water. The large ε_s for ice-Ih can be attributed to hydrogen-bond rearrangements under an external electric field. The structure of ice-Ih satisfies the ice rules: each water molecule in ice will form four hydrogen bonds with its first-solvation-shell water molecules. The water will serve as a hydrogen acceptor in two of the hydrogen bonds and a hydrogen donor in the other two. For the infinite bulk phase of ice-Ih, there are infinite hydrogen-bond arrangements that satisfy the ice rules. The many possible hydrogen-bond arrangements give rise to the Pauling entropy. While Pauling assumed that all the hydrogen-bond arrangements are degenerate, the configuration energies of various proton arrangements are not identical. In order to determine ε_s for ice-Ih, these hydrogen-bond arrangements have to be sampled.

Below the melting temperature, the relaxation time of the hydrogen-bond arrangements is much larger than typical time scale accessible to molecular dynamics simulations. While ε_s for ice-Ih has been determined with Monte-Carlo, it has only recently been calculated in the framework of molecular dynamics with the electrostatic switching method [60]. However, direct application of the electrostatic switching method in electronic-structure-based MD is not feasible. In this work, we calculate DFT-level ε_s of ice-Ih through the ab initio FEP approach by developing a force field for FEP with the AFM method. We choose the Perdew–Wang 91 (PW-91) [65] exchange-correlation functional to provide the electronic-structure energy and forces under Kohn–Sham DFT [66].

Before the ab initio FEP calculation was performed, a customized force field was developed to achieve the best sampling for the ab initio FEP procedure. In order to develop such a problem-specific force field, the sampling step in AFM was performed at simulation conditions identical to those needed for the ab initio FEP study. In both cases, we used an orthorhombic simulation box with the lattice vectors $a = b = 9.06$ Å, $c = 14.72$ Å. The angle between lattice vectors a and b is 120°. The supercell contains 32 molecules with a volume of 1,040.96 Å^3 (Fig. 1). The sampling was performed with the electrostatic switching method. All other parameters for the electrostatic

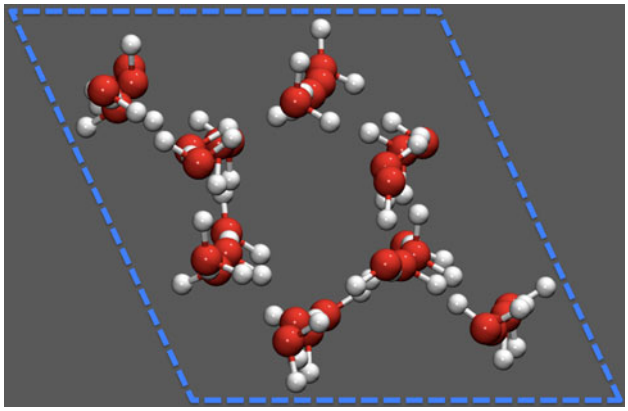

Fig. 1 An ice configuration with 32 water molecules in orthorhombic periodic *box* viewed from the *top*. The *dotted line* indicates simulation *box* boundaries

switching calculation were taken from our previous work [30]. The sampling was performed at 253.15 K.

A total of 300 configurations were generated for each generation of AFM. As mentioned previously, the PW-91 exchange-correlation functional was used to calculate reference forces. Since DFT is fairly inexpensive, we are able to model the whole box with DFT instead of relying on QM/MM.

The reference forces were obtained using the Vienna Ab-initio Simulation Package (VASP) [67–70], along with the generalized gradient approximation PW-91 exchange-correlation functional [65]. The core electrons are approximated with the Vanderbilt ultrasoft pseudo-potentials [71]. A plane wave basis set with a kinetic energy cutoff of 500 eV was used. The electronic energies are required to converge to 10^{-5} eV before the self-consistent iterations were allowed to terminate. Atomic forces were calculated with the Hellman-Feynman theorem [72]. Integration of the electronic distribution at the Fermi level was facilitated by the use of first order Methfessel–Paxton smearing [73] with a smearing width of 0.005 eV. Sampling of the first Brillouin zone was performed using a discrete 3 × 3 × 2 Monkhorst–Pack *k*-point mesh [74].

The energy expression for the AFM force field is the 4-point flexible model published previously [30], with charges only on hydrogen atoms and the off-atom virtual site. The importance of each term in this force field has been established with AFM. Only the terms that most significantly reduce the force RMSE were included [30, 32]. This force field contains 14 parameters; only 12 of the 14 parameters were optimized in this work. The r_c and M-site *a* parameters were taken from our previous work and not reoptimized.

Due to the use of periodic boundary conditions, our current force-matching program does not support fitting Columbic terms with SVD when the Ewald summation method [75, 76] is used to model long-range electrostatics. Therefore, in this work, we used the simplex method in the fitting step [77]. Since simplex is a nonlinear optimization algorithm, we do not need to fit charge products as done previously. The atomic partial charges were fit directly. Since charge products were not being fit, the last term of Eq. 1 was omitted.

In order to avoid being trapped in a local minimum, three random trial moves are performed after simplex converges[1] by perturbing each of the converged force field parameters. This is accomplished by multiplying each parameter by a random number from a uniform distribution between 0.9 and 1.1, inclusive. Additional simplex optimizations are performed starting from these perturbed initial guesses. If the additional simplex optimizations find a better minimum, the above process is repeated from the best minimum. The simplex iterations will terminate if no new minimum can be found after the random perturbations. We will refer to this variant of simplex method as simplex with random perturbations. The initial guess for the very first simplex optimization is always the parameters from the previous generation of AFM. In our studies, the perturbed guesses occasionally lead to a lower minimum. The optimal RMSE obtained by the simplex with random perturbation is in the same range as the RMSEs produced previously with SVD. Thus, we have good reasons to believe the true global minimum for the objective functions can be obtained with our method.

The ice-Ih ε_s was calculated by the fluctuation-dissipation theorem with the formula

$$\varepsilon_s = \varepsilon_0 + \frac{4\pi}{3Vk_BT}\left(\langle M^2\rangle - \langle M\rangle^2\right) \tag{5}$$

where V is the volume and M is the dipole moment of the box. The electronic contribution to the dielectric constant of 1.78 was used as ε_0 [64]. For determination of the PW91 ε_s, the dipole fluctuation and average dipole moments were determined following the standard FEP method using

$$\langle M\rangle_A = \frac{\left\langle M_i \cdot e^{-(U_A-U_F)/k_BT}\right\rangle_F}{\left\langle e^{-(U_A-U_F)/k_BT}\right\rangle_F}, \tag{6}$$

and

$$\langle M^2\rangle_A = \frac{\left\langle M_i^2 \cdot e^{-(U_A-U_F)/k_BT}\right\rangle_F}{\left\langle e^{-(U_A-U_F)/k_BT}\right\rangle_F}, \tag{7}$$

[1] It is well known that the simplex algorithm occasionally suffers from false termination and should always be restarted from the converged parameters to make sure no further optimization is possible. In this work, we will not consider a simplex algorithm converged unless such a restart has been performed to verify that the final parameters are indeed a minimum.

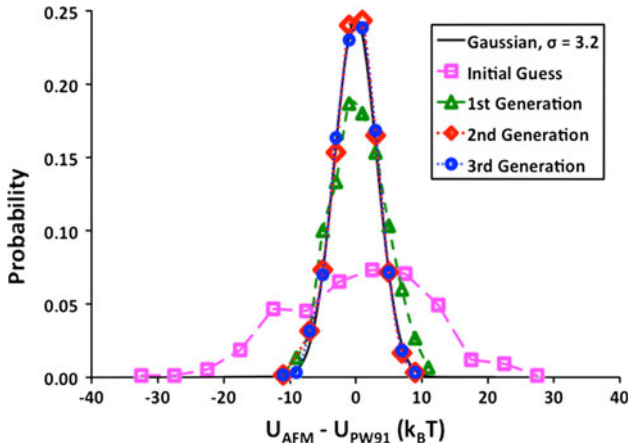

Fig. 2 Relative energy difference distribution for each generation of AFM. The medians of PW-91 and force field energies are set to be zero. A number of 300 configurations from each generation were used to produce this figure. The final generation was fit to a Gaussian distribution (*black curve*) with a standard deviation of 3.2 k_BT. The area *below* each curve was normalized to one

such that the ab initio dipole moment M of configuration i is reweighed according to the potential energy difference $U_A - U_F$, where U_F is the force field energy and U_A is the DFT energy.

The DFT dipole moment was determined using the Bader's atoms-in-molecules approach [78] via a modified version of the *Bader* module [79–81]. Both the partial charge contribution and the first moment contribution to the dipole moment were calculated [82, 83]. The molecular dipole moment determined by this method does not depend on the partitioning between different atoms of the same molecule and is rigorously correct as long as the Bader surfaces between molecules are properly determined [82, 84]. Our calculation with a single water in a periodic box produced a dipole moment of 1.84 D following this approach, in excellent agreement with the experimental dipole moment of water [85].

The initial guess for AFM was the BLYP-SP$_f$ model published by Wang et al [34]. Figure 2 plots the REDD for each generation of AFM. We note that only the PW-91 forces were fitted in AFM; the relative energies were only used to calculate the REDD and not fitted. As mentioned previously, the medians of the energies were set to zero. If the force field created by AFM correctly reproduces the PW-91 relative energies, the distribution in Fig. 2 will be a δ function centered at zero. It is clear from Fig. 2 that standard deviation of the REDD, the relative energy RMSE, quickly reduces for each generation of AFM and converges to 1.6 kcal/mol after generation 2. The fast convergence of AFM was observed in all previous works [30–34]. After convergence, the relative energy RMSE of 1.6 kcal/mol is 3.2 k_BT at the sampling temperature of 253.15 K. This is a significant improvement over the initial guess, which gives a relative energy RMSE of 4.9 kcal/mol (9.7 k_BT) for the REDD.

Table 1 Parameters for the PW91-Ice$_f$ force field

Parameter	Value	Parameter	Value
Q_M (e)	−1.484	r_e (Å)	0.964
q_H (e)	0.742	k_2 (kcal/(mol Å^2))	1,170
A_{OO} (kcal/mol)	239,000	k_3 (kcal/(mol Å^3))	−4,540
α (Å^{-1})	4.06	k_4 (kcal/(mol Å^4))	7,610
C_{OO} (kcal Å^6/mol)	1,020	θ_e (°)	106.73
A_4 (kcal Å^4/mol)	82.5	k_θ (kcal/(mol rad^2))	81.06

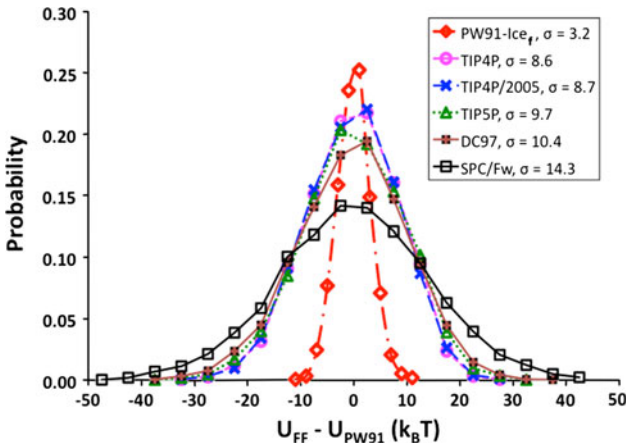

Fig. 3 Relative energy difference distribution of the PW91-ice$_f$ force field developed with AFM and several off-the-shelf models. The medians of PW-91 energies (U_{PW91}) and force field energies (U_{FF}) are set to be zero. A number of 3,600 configurations sampled with PW91-ice$_f$ are used for each force field. The standard deviation, σ, in unit of k_BT is reported with the legend. The area *below* each curve was normalized to one

The converged AFM force field will be referred to as PW91-ice$_f$. The parameters for this potential are summarized in Table 1. A number of 3,600 configurations are obtained with the PW91-ice$_f$ potential. The REDD for the 3,600 configurations is plotted in Fig. 3; the relative energy RMSE for these configurations is 1.59 kcal/mol (3.2 k_BT), in perfect agreement with that estimated with the 300 configurations. The REDDs for selected off-the-shelf models, Simple Point Charge/Flexible Wu (SPC/FW) [86], Transferable Intermolecular Potential 4 Point (TIP4P) [87], TIP4P/2005 [88], Dang-Chang 97 (DC97) [89], and Transferable Intermolecular Potential 5 Point (TIP5P) [90] are also reported in this figure. SPC/FW is a flexible 3-site model. TIP4P and TIP4P/2005 are rigid 4-site models with the TIP4P/2005 model specifically optimized to reproduce the melting temperature of ice-Ih and heat of vaporization of liquid water. DC97 is a polarizable but rigid 4-site model. TIP5P is a rigid 5-site model fit to reproduce the density

maximum of water. Compared with the customized force field PW91-ice$_f$, the off-the-shelf models perform significantly worse in reproducing the PW91 relative energies. The TIP4P and TIP4P/2005 models give relative energy RMSEs of 4.3 and 4.4 kcal/mol, respectively. The DC97 model produced a relative energy RMSE of 5.2 kcal/mol. The fact that the polarizable DC97 model is slightly worse than the non-polarizable TIP4P is somewhat surprising. TIP5P produces a relative energy RMSE of 4.9 kcal/mol. The TIP5P model being slightly worse than TIP4P is not surprising. Although the ice-Ih melting temperature of TIP5P water is close to the experimental value of 273 K, it has been established that TIP5P predicts ice-Ih to be metastable. The most stable phase for the TIP5P model at 273 K is ice II [91, 92]. The three-point SPC/FW model performs significantly worse, giving a relative energy RMSE of 7.2 kcal/mol. This is in agreement with the common understanding that a 4-site model is generally better than a 3-site model at describing the solid phases of water.

As mentioned previously, the weight of each micro-state in ab initio FEP depends exponentially on the relative energy difference. The AFM model produces a standard deviation of 3.2 k_BT for the REDD, which is significantly narrower than the 8.6 k_BT standard deviation of the best off-the-shelf model tested. The convergence of the FEP calculation is thereby improved by approximately a factor of $e^{5.4} = 221$ with the AFM force field. We note the development of the AFM potential only incurred a fraction of the cost of the ab initio FEP.

The ε_s of PW-91 ice-Ih was calculated to be 80 ± 4, slightly lower than the experimental value of 99.4 [85]. The conclusion that PW-91 underestimates ice-Ih ε_s by about 20% supports the general belief that common DFT functions are insufficient for modeling the strongly hydrogen-bonded ice and water [93–95]. DFT tends to predict a liquid water structure that is too ordered under constant volume conditions [96–98]. At the same time, popular DFT functionals overestimate the ice-Ih melting temperature [99–101], underestimate liquid water density [93, 102], and overestimate ice density [103, 104].

Figure 4 reports the dipole moments of individual water molecules predicted by PW-91, the PW91-ice$_f$ force field, and the DC97 potential. The average water dipole moment is 2.55 D according to PW-91, which is also about 20% smaller than an estimate of 3.09 D based on a recent self-consistent induction model fit to experimental multiple moments and polarizability [105]. Since the ε_s, scales linearly with the square of dipole moments, it is possible that the 3.09 D estimate is too high. Given that ice-Ih is a crystal, the large variance of the water dipole moment distribution is noteworthy. As seen in Fig. 4, the most polarized water has a dipole moment of about 3.1 D, and the least polarized water only has a dipole moment close to

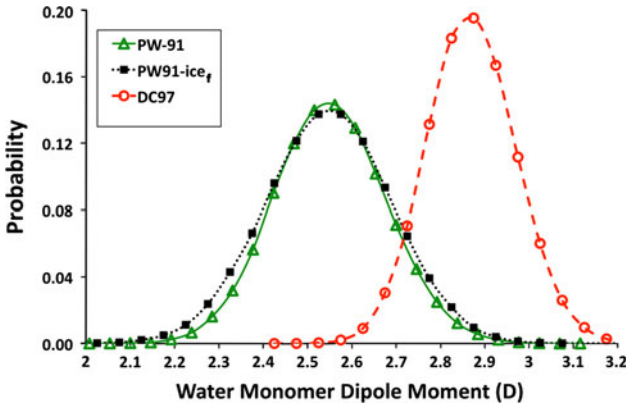

Fig. 4 Distribution of water monomer dipole moments. The area *below* the curve was normalized to one

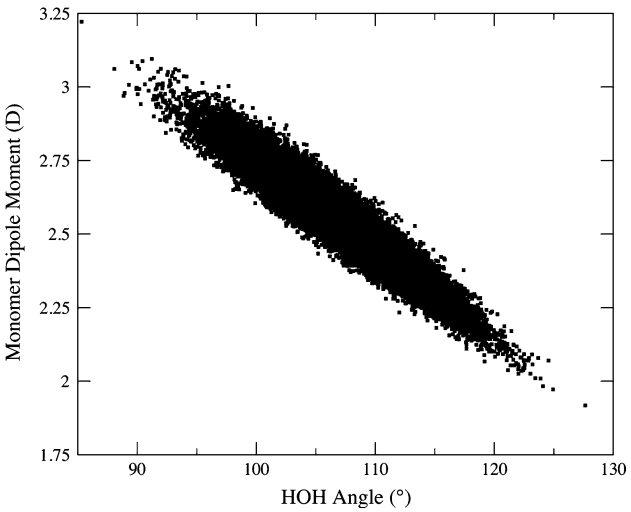

Fig. 5 *Scatter plot* showing the correlation of the dipole moment and the HOH angle for each water molecule. Each water molecule from the 3,600 ice configurations is represented as a point in this scatter plot

2.0 D. The PW91-ice$_f$ force field provides a very similar distribution of dipole moments centered around 2.55 D. This is very surprising considering PW91-ice$_f$ is not a polarizable model. Figure 5 shows a scatter plot of each water's dipole moment versus its HOH angle. Each water molecule in the 3,600 configurations is represented as a point in this figure. It is clear from Fig. 5 that the HOH angle is strongly anti-correlated with the dipole moment, allowing a flexible model to reproduce a dipole moment distribution similar to that of PW-91 waters by varying its angle.

The DC-97 model predicts a larger average dipole moment at 2.87 D but produced a smaller ε_s of 75 ± 1 at 253.15 K. This is caused by DC-97 not producing the correct ensemble weight for the various micro-states. The DC97 water model has a monomer polarizability of

1.44 Å^3, which is identical to the experimental polarizability of water in gas phase. Since the PW-91 polarizability of water in gas phase was calculated to be 1.55 Å^3[104], it is somewhat surprising to see the induced dipole moment for water in ice-Ih is actually lower for PW-91.

We also calculated the ice-Ih ε_s using the AFM-ice model without FEP. With the same 3,600 configurations, the ε_s was determined to be 56.4 ± 0.4. The error bar is noticeably smaller. This is due to the finite width of the REDD. The FEP weight makes the statistics poorer with the reweighting. The ε_s estimate with the PW91-ice$_f$ force field is significantly lower than the PW-91 functional.

Two contributions cause the ε_s estimated with the force field to be different from that obtained using FEP. The first contribution is due to slightly different Boltzmann weight in the equilibrium ensemble. The second contribution is from the difference in box dipole moments predicted by the PW-91 and the unpolarizable force field. We will refer to the two contributions as the Boltzmann contribution and the polarization contribution.

In order to disentangle the two contributions, the reweighted PW91-ice$_f$ ε_s is reported in Table 2. This quantity was obtained by using the force field dipole moment but reweight each configuration to have the same Boltzmann weight as the DFT method. The reweighted PW91-ice$_f$ model predicted an ε_s of 76 ± 7, which is in good agreement with the PW-91 estimate. The contribution due to polarization is thus only 4. Figure 6 reports a scatter plot where each point is one of the *x*, *y*, and *z* components of the dipole moment vector. The *x*-axis of each point is the PW-91 dipole moment component of the box and y-axis is the corresponding component of the PW91-ice$_f$ dipole moment. All of the points are very close to the diagonal line, indicating the PW91-ice$_f$ model is doing a very good job at reproducing the PW-91 box dipole moment. The RMSE of the dipole moment component is about 1.1 D, which is significantly smaller than the 13 D root mean square dipole moment for each component of the simulation box. Not surprisingly, with the DFT dipole moments and the Boltzmann weight of the force field, an ε_s of 58.3 is produced. Compared with a value of 56.4 obtained with the force field dipole moments, the polarization contribution is again negligibly small.

It is worth commenting on the small 32-water box size used in this study. Potentially a finite size effect could skew the ε_s measured with the DFT method. It has been established previously that a 128-water box predicts the same ε_s as a 300-water box with a non-polarizable model [60]. We reinvestigated the finite size effect with the DC97 polarizable model. The ε_s calculated with the 32-water box is 75 ± 1, while 300 configurations using a 300-water box give a ice-Ih ε_s of 74 ± 1 at the same temperature. This indicates that a 32-water box is indeed sufficient.

Table 2 Static dielectric constants of ice-Ih for PW-91 and MD force fields at 253.15 K

	PW-91	PW91-ice$_f$	Reweighted PW91-ice$_f$	DC97
ε_s	80 ± 4	56.4 ± 0.4	76 ± 7	75 ± 1

The experimental ε_s is 99.4

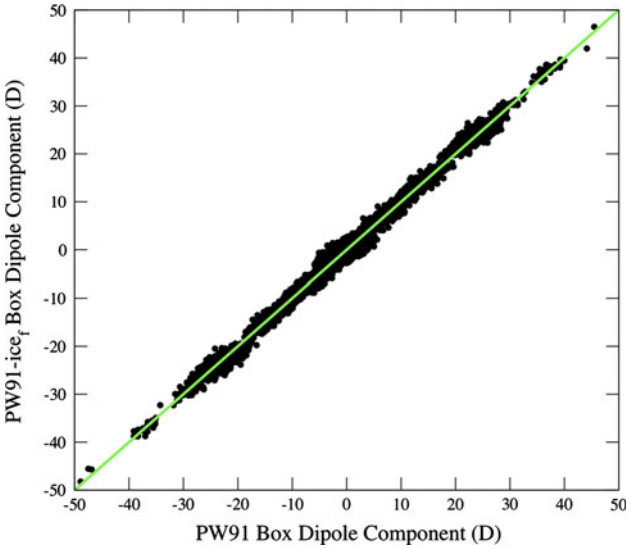

Fig. 6 *Box* dipole moment component scatter plot. Each component of the dipole moment vector is plotted separately. The *y* axis is dipole moment components produced by the PW91-ice$_f$ force field, the *x* axis is the dipole moment components calculated with PW-91. The root mean square error of the dipole moment components is 1.1 D

In our previous work, bifurcated hydrogen-bond defects were reported in ice-Ih at temperature as low as 200 K. It has been argued whether such a hydrogen-bond defect could be an artifact of the force field [60]. With the more accurate PW91-ice$_f$ model, one hydrogen-bond defect was detected from the 3,600 configurations sampled at 253.15 K, indicating such hydrogen-bond defects are likely to be real.

5 Summary

Ab initio FEP is a powerful method for obtaining electronic-structure-quality thermodynamic properties with sampling performed by inexpensive MM force fields. It is demonstrated in this work that creating a customized force field for ab initio FEP with AFM significantly accelerates the convergence of ab initio FEP, thus making ab initio FEP an even more powerful method. The PW-91 ε_s of ice-Ih was calculated through ab initio FEP. The customized force field created with AFM produced a REDD with a standard deviation of 1.6 kcal/mol. This compares favorably with a standard deviation of 4.3 kcal/mol at 253.15 K

produced by the best off-the-shelf model tested, TIP4P. Such an improvement of the REDD makes sampling 220 times more efficient with the AFM force field than with TIP4P for ab initio FEP.

In this work, the number of electronic-structure calculations used for the development of the force field is a small fraction of the number of electronic-structure calculations used for converging the ab initio FEP. The savings from improved sampling decisively outweighs the cost associated with developing the AFM force field.

The PW-91 method predicts a gas phase water dipole moment of 1.84 D, in good agreement with experimental measurement. The PW-91 average water dipole moment in ice-Ih is predicted to be 2.55 D. The PW-91 ε_s for ice-Ih is determined to be 80 ± 4, underestimating the experimental estimate by about 20%. It is a pleasant surprise that the non-polarizable force field developed through AFM is able to reproduce the dipole moment distribution for the PW-91 reference method for the ice-Ih configurations. This is achieved through the flexible HOH bond.

Acknowledgments This work is supported by NSF CAREER award CHE0748628. The computer resource for this study is provided by the National Center for Supercomputing Applications under grant TG-CHE070060 and by the Boston University Center for Scientific Computing.

References

1. Head-Gordon M, Pople JA (1988) A method for two-electron Gaussian integral and integral derivative evaluation using recurrence relations. J Chem Phys 89(9):5777–5786
2. Moller C, Plesset MS (1934) Note on an approximation treatment for many-electron systems. Phys Rev 46(7):618
3. Saebo S, Almlof J (1989) Avoiding the integral storage bottleneck in LCAO calculations of electron correlation. Chem Phys Lett 154(1):83–89
4. Frisch MJ, Head-Gordon M, Pople JA (1990) A direct MP2 gradient method. Chem Phys Lett 166(3):275–280
5. Krishnan R, Pople JA (1978) Approximate fourth-order perturbation theory of the electron correlation energy. Int J Quantum Chem 14(1):91–100. doi:10.1002/qua.560140109
6. Raghavachari K, Pople JA (1981) Calculation of one-electron properties using limited configuration interaction techniques. Int J Quantum Chem 20(5):1067–1071. doi:10.1002/qua.560200503
7. Pople JA, Seeger R, Krishnan R (1977) Variational configuration interaction methods and comparison with perturbation theory. Int J Quantum Chem 12(S11):149–163. doi:10.1002/qua.560120820
8. Krishnan R, Schlegel HB, Pople JA (1980) Derivative studies in configuration—interaction theory. J Chem Phys 72(8):4654–4655
9. Cizek J (1966) On the correlation problem in atomic and molecular systems. calculation of wavefunction components in Ursell-type expansion using quantum-field theoretical methods. J Chem Phys 45(11):4256–4266
10. Kummel HG (2003) A biography of the coupled cluster method. Int J Modern Phys B 17(28):14
11. Head-Gordon M, Head-Gordon T (1994) Analytic MP2 frequencies without fifth-order storage. Theory and application to bifurcated hydrogen bonds in the water hexamer. Chem Phys Lett 220(1–2):122–128
12. Bernholdt DE, Harrison RJ (1996) Large-scale correlated electronic structure calculations: the RI-MP2 method on parallel computers. Chem Phys Lett 250(5–6):477–484
13. Feyereisen M, Fitzgerald G, Komornicki A (1993) Use of approximate integrals in ab initio theory. An application in MP2 energy calculations. Chem Phys Lett 208(5–6):359–363
14. Schutz M, Hetzer G, Werner H-J (1999) Low-order scaling local electron correlation methods. I. Linear scaling local MP2. J Chem Phys 111(13):5691–5705
15. Hetzer G, Schutz M, Stoll H, Werner H-J (2000) Low-order scaling local correlation methods II: splitting the Coulomb operator in linear scaling local second-order Moller–Plesset perturbation theory. J Chem Phys 113(21):9443–9455
16. Lee MS, Maslen PE, Head-Gordon M (2000) Closely approximating second-order M[o-slash]ller–Plesset perturbation theory with a local triatomics in molecules model. J Chem Phys 112(8):3592–3601
17. Parr RG, Yang W (1994) Density-functional theory of atoms and molecules. Oxford University Press, New York
18. Kohn W, Sham LJ (1965) Self-consistent equations including exchange and correlation effects. Phys Rev 140(4A):A1133
19. Parr RG, Yang WT (1995) Density-functional theory of the electronic-structure of molecules. Annu Rev Phys Chem 46:701–728
20. Bowler DR, Miyazaki T (2010) Calculations for millions of atoms with density functional theory: linear scaling shows its potential. J Phys Condens Matter 22(7):074207
21. Shimojo F, Kalia RK, Nakano A, Vashishta P (2005) Embedded divide-and-conquer algorithm on hierarchical real-space grids: parallel molecular dynamics simulation based on linear-scaling density functional theory. Comput Phys Commun 167(3):151–164
22. Nakano A, Kalia RK, Nomura K-I, Sharma A, Vashishta P, Shimojo F, van Duin ACT, Goddard WA, Biswas R, Srivastava D (2007) A divide-and-conquer/cellular-decomposition framework for million-to-billion atom simulations of chemical reactions. Comput Mater Sci 38(4):642–652
23. Bowler DR et al (2008) Introductory remarks: linear scaling methods. J Phys Condens Matter 20(29):290301
24. Goedecker S (1999) Linear scaling electronic structure methods. Rev Modern Phys 71(4):1085
25. Carter EA (2008) Challenges in modeling materials properties without experimental input. Science 321(5890):800–803. doi:10.1126/science.1158009
26. Smargiassi E, Madden PA (1994) Orbital-free kinetic-energy functionals for first-principles molecular dynamics. Phys Rev B 49(8):5220
27. Wang YA, Govind N, Carter EA (1999) Orbital-free kinetic-energy density functionals with a density-dependent kernel. Phys Rev B 60(24):16350
28. Gavini V, Bhattacharya K, Ortiz M (2007) Quasi-continuum orbital-free density-functional theory: a route to multi-million atom non-periodic DFT calculation. J Mech Phys Solids 55(4):697–718
29. Wang YA, Carter EA (2002) Theoretical methods in condensed phase chemistry, vol 5. Kluwer, Dordrecht
30. Akin-Ojo O, Wang F (2011) The quest for the best nonpolarizable water model from the adaptive force matching method. J Comput Chem 32(3):453–462. doi:10.1002/jcc.21634
31. Akin-Ojo O, Song Y, Wang F (2008) Developing ab initio quality force fields from condensed phase quantum-mechanics/molecular-mechanics calculations through the adaptive force matching method. J Chem Phys 129(6):064108
32. Akin-Ojo O, Wang F (2009) Improving the point-charge description of hydrogen bonds by adaptive force matching. J Phys Chem B 113(5):1237–1240. doi:10.1021/jp809324x

33. Wei D, Song Y, Wang F (2011) A simple molecular mechanics potential for mum scale graphene simulations from the adaptive force matching method. J Chem Phys 134(18):184704
34. Wang F, Akin-Ojo O, Pinnick ER, Song Y (2011) Approaching Post-Hartree–Fock quality potential energy surfaces with simple pair-wise expressions: parameterizing point-charge based force fields for liquid water using the adaptive force matching method. Mol Simul 37:591
35. Sakane S, Yezdimer EM, Liu W, Barriocanal JA, Doren DJ, Wood RH (2000) Exploring the ab initio/classical free energy perturbation method: the hydration free energy of water. J Chem Phys 113(7):2583–2593
36. Wesolowski T, Warshel A (1994) Ab initio free energy perturbation calculations of solvation free energy using the frozen density functional approach. J Phys Chem 98(20):5183–5187. doi:10.1021/j100071a003
37. Muller RP, Warshel A (1995) Ab initio calculations of free energy barriers for chemical reactions in solution. J Phys Chem 99(49):17516–17524. doi:10.1021/j100049a009
38. Wood RH, Yezdimer EM, Sakane S, Barriocanal JA, Doren DJ (1999) Free energies of solvation with quantum mechanical interaction energies from classical mechanical simulations. J Chem Phys 110(3):1329–1337
39. Ischtwan J, Collins MA (1994) Molecular potential energy surfaces by interpolation. J Chem Phys 100(11):8080–8088
40. Piquemal J-P, Marquez A, Parisel O, Giessner-Prettre C (2005) A CSOV study of the difference between HF and DFT intermolecular interaction energy values: the importance of the charge transfer contribution. J Comput Chem 26(10):1052–1062. doi:10.1002/jcc.20242
41. Kristyán S, Pulay P (1994) Can (semi)local density functional theory account for the London dispersion forces? Chem Phys Lett 229(3):175–180
42. Burnham CJ, Xantheas SS (2002) Development of transferable interaction models for water. III. Reparametrization of an all-atom polarizable rigid model (TTM2-R) from first principles. J Chem Phys 116(4):1500–1510
43. Basch H, Stevens WJ (1995) Hydrogen bonding between aromatics and cationic amino groups. J Mol Struct THEOCHEM 338(1–3):303–315
44. Li H, Gordon MS, Jensen JH (2006) Charge transfer interaction in the effective fragment potential method. J Chem Phys 124(21):214108
45. Reed AE, Curtiss LA, Weinhold F (1988) Intermolecular interactions from a natural bond orbital, donor-acceptor viewpoint. Chem Rev 88(6):899–926. doi:10.1021/cr00088a005
46. Murdachaew G, Mundy CJ, Schenter GK (2010) Improving the density functional theory description of water with self-consistent polarization. J Chem Phys 132(16):164102
47. Chang DT, Schenter GK, Garrett BC (2008) Self-consistent polarization neglect of diatomic differential overlap: application to water clusters. J Chem Phys 128(16):164111
48. Tsuzuki S, Luthi HP (2001) Interaction energies of van der Waals and hydrogen bonded systems calculated using density functional theory: assessing the PW91 model. J Chem Phys 114(9):3949–3957
49. Gresh N, Cisneros GA, Darden TA, Piquemal J-P (2007) Anisotropic, polarizable molecular mechanics studies of inter- and intramolecular interactions and ligand-macromolecule complexes. A bottom–up strategy. J Chem Theory Comput 3(6):1960–1986. doi:10.1021/ct700134r
50. Piquemal J-P, Chelli R, Procacci P, Gresh N (2007) Key role of the polarization anisotropy of water in modeling classical polarizable force fields. J Phys Chem A 111(33):8170–8176. doi:10.1021/jp072687g
51. Golub G, Kahan W (1965) Calculating the singular values and pseudo-inverse of a matrix. J Soc Ind Appl Math Se B Numer Anal 2(2):205–224
52. Trefethen LN, Bau D (1997) Numerical linear algebra. Society for Industrial and Applied Mathematics, Philadelphia
53. Izvekov S, Parrinello M, Burnham CJ, Voth GA (2004) Effective force fields for condensed phase systems from ab initio molecular dynamics simulation: a new method for force-matching. J Chem Phys 120(23):10896–10913
54. Zwanzig RW (1954) High-temperature equation of state by a perturbation method. I. Nonpolar gases. J Chem Phys 22(8):1420–1426
55. Dang LX, Pearlman DA, Kollman PA (1990) Why do A.T base pairs inhibit Z-DNA formation? Proc Natl Acad Sci 87(12):4630–4634
56. Dang LX, Merz KM, Kollman PA (1989) Free energy calculations on protein stability: Thr-157 Val-157 mutation of T4 lysozyme. J Am Chem Soc 111(22):8505–8508. doi:10.1021/ja00204a027
57. Allen MP, Tildesley DJ (1999) Computer simulation of liquids. Clarendon Press, Oxford
58. Wood RH, Dong H (2011) Communication: combining non-Boltzmann sampling with free energy perturbation to calculate free energies of hydration of quantum models from a simulation of an approximate model. J Chem Phys 134(10):101101
59. Rick SW, Haymet ADJ (2003) Dielectric constant and proton order and disorder in ice Ih: Monte Carlo computer simulations. J Chem Phys 118(20):9291–9296
60. Lindberg GE, Wang F (2008) Efficient sampling of ice structures by electrostatic switching. J Phys Chem B 112(20):6436–6441. doi:10.1021/jp800736t
61. Leach AR (1996) Molecular modelling: principles and applications. Longman, Harlow
62. Rahman A, Stillinger FH (1972) Proton distribution in ice and the Kirkwood correlation factor. J Chem Phys 57(9):4009–4017
63. Aragones JL, MacDowell LG, Vega C (2010) Dielectric constant of ices and water: a lesson about water interactions. J Phys Chem A 115(23):5745–5758. doi:10.1021/jp105975c
64. Lu D, Gygi F, Galli G (2008) Dielectric properties of ice and liquid water from first-principles calculations. Phys Rev Lett 100(14):147601
65. Perdew JP, Wang Y (1992) Accurate and simple analytic representation of the electron-gas correlation energy. Phys Rev B 45(23):13244
66. Perdew JP, Chevary JA, Vosko SH, Jackson KA, Pederson MR, Singh DJ, Fiolhais C (1993) Erratum: Atoms, molecules, solids, and surfaces: applications of the generalized gradient approximation for exchange and correlation. Phys Rev B 48(7):4978
67. Kresse G, Hafner J (1993) Ab initio molecular dynamics for liquid metals. Phys Rev B 47(1):558
68. Kresse G, Furthmüller J (1996) Efficient iterative schemes for ab initio total-energy calculations using a plane-wave basis set. Phys Rev B 54(16):11169
69. Kresse G, Hafner J (1994) Ab initio molecular-dynamics simulation of the liquid-metal–amorphous-semiconductor transition in germanium. Phys Rev B 49(20):14251
70. Kresse G, Furthmüller J (1996) Efficiency of ab-initio total energy calculations for metals and semiconductors using a plane-wave basis set. Comput Mater Sci 6(1):15–50
71. Vanderbilt D (1985) Optimally smooth norm-conserving pseudopotentials. Phys Rev B 32(12):8412
72. Feynman RP (1939) Forces in molecules. Phys Rev 56(4):340
73. Methfessel M, Paxton AT (1989) High-precision sampling for Brillouin-zone integration in metals. Phys Rev B 40(6):3616
74. Monkhorst HJ, Pack JD (1976) Special points for Brillouin-zone integrations. Phys Rev B 13(12):5188

75. Darden T, York D, Pedersen L (1993) Particle mesh Ewald: an N·log(N) method for Ewald sums in large systems. J Chem Phys 98(12):10089–10092. doi:10.1063/1.464397
76. Essmann U, Perera L, Berkowitz ML, Darden T, Lee H, Pedersen LG (1995) A smooth particle mesh Ewald method. J Chem Phys 103(19):8577–8593. doi:10.1063/1.470117
77. Press WH (2007) Numerical recipes: the art of scientific computing. Cambridge University Press, New York
78. Bader RFW (1990) Atoms in molecules: a quantum theory. Clarendon Press, Oxford
79. Tang W et al (2009) A grid-based Bader analysis algorithm without lattice bias. J Phys Condens Matter 21(8):084204
80. Henkelman G, Arnaldsson A, Jûnsson H (2006) A fast and robust algorithm for Bader decomposition of charge density. Comput Mater Sci 36(3):354–360
81. Sanville E, Kenny SD, Smith R, Henkelman G (2007) Improved grid-based algorithm for Bader charge allocation. J Comput Chem 28(5):899–908. doi:10.1002/jcc.20575
82. Bader RFW, Larouche A, Gatti C, Carroll MT, MacDougall PJ, Wiberg KB (1987) Properties of atoms in molecules: dipole moments and transferability of properties. J Chem Phys 87(2): 1142–1152. doi:10.1063/1.453294
83. Gatti C, Silvi B, Colonna F (1995) Dipole moment of the water molecule in the condensed phase: a periodic Hartree–Fock estimate. Chem Phys Lett 247(1–2):135–141. doi:10.1016/0009-2614(95)01190-0
84. Bader RFW, Matta CF (2001) Properties of atoms in crystals: dielectric polarization. Int J Quantum Chem 85(4–5):592–607. doi:10.1002/qua.1540
85. Haynes WM (2011) CRC handbook of chemistry and physics. Taylor and Francis, London
86. Wu Y, Tepper HL, Voth GA (2006) Flexible simple point-charge water model with improved liquid-state properties. J Chem Phys 124(2):024503. doi:10.1063/1.2136877
87. Jorgensen WL, Chandrasekhar J, Madura JD, Impey RW, Klein ML (1983) Comparison of simple potential functions for simulating liquid water. J Chem Phys 79(2):926–935
88. Abascal JLF, Vega C (2005) A general purpose model for the condensed phases of water: TIP4P/2005. J Chem Phys 123(23): 234505
89. Dang LX, Chang T-M (1997) Molecular dynamics study of water clusters, liquid, and liquid–vapor interface of water with many-body potentials. J Chem Phys 106(19):8149–8159
90. Mahoney MW, Jorgensen WL (2000) A five-site model for liquid water and the reproduction of the density anomaly by rigid, nonpolarizable potential functions. J Chem Phys 112(20): 8910–8922
91. Aragones JL, Noya EG, Abascal JLF, Vega C (2007) Properties of ices at 0 K: a test of water models. J Chem Phys 127(15):154518
92. Vega C, Abascal JLF, Conde MM, Aragones JL (2009) What ice can teach us about water interactions: a critical comparison of the performance of different water models. Faraday Discuss 141:251–276
93. Schmidt J, VandeVondele J, Kuo IFW, Sebastiani D, Siepmann JI, Hutter J, Mundy CJ (2009) Isobaric, isothermal molecular dynamics simulations utilizing density functional theory: an assessment of the structure and density of water at near-ambient conditions. J Phys Chem B 113(35):11959–11964. doi:10.1021/jp901990u
94. McGrath MJ, Siepmann JI, Kuo IFW, Mundy CJ, VandeVondele J, Hutter J Jr, Mohamed F, Krack M (2005) Simulating fluid-phase equilibria of water from first principles. J Phys Chem A 110(2):640–646. doi:10.1021/jp0535947
95. Sprik M, Hutter J, Parrinello M (1996) Ab initio molecular dynamics simulation of liquid water: comparison of three gradient-corrected density functionals. J Chem Phys 105(3):1142–1152
96. Lee H-S, Tuckerman ME (2006) Structure of liquid water at ambient temperature from ab initio molecular dynamics performed in the complete basis set limit. J Chem Phys 125(15):154507
97. Grossman JC, Schwegler E, Draeger EW, Gygi F, Galli G (2004) Towards an assessment of the accuracy of density functional theory for first principles simulations of water. J Chem Phys 120(1):300–311
98. Schwegler E, Grossman JC, Gygi F, Galli G (2004) Towards an assessment of the accuracy of density functional theory for first principles simulations of water. II. J Chem Phys 121(11):5400–5409
99. Yoo S, Zeng XC, Xantheas SS (2009) On the phase diagram of water with density functional theory potentials: the melting temperature of ice I_h with the Perdew–Burke–Ernzerhof and Becke–Lee–Yang–Parr functionals. J Chem Phys 130(22):221102
100. Yoo S, Xantheas SS (2011) Communication: the effect of dispersion corrections on the melting temperature of liquid water. J Chem Phys 134(12):121105
101. Schwegler E, Sharma M, Gygi F, Galli G (2008) Melting of ice under pressure. Proc Natl Acad Sci 105(39):14779–14783. doi:10.1073/pnas.0808137105
102. McGrath MJ, Siepmann JI, Kuo I-FW, Mundy CJ (2006) Vapor–liquid equilibria of water from first principles: comparison of density functionals and basis sets. Mol Phys Int J Interface Between Chem Phys 104(22):3619–3626
103. Fortes AD, Wood IG, Brodholt JP, Vocadlo L (2003) Ab initio simulation of the ice II structure. J Chem Phys 119(8):4567–4572
104. Leung K, Rempe SB (2006) Ab initio rigid water: effect on water structure, ion hydration, and thermodynamics. Phys Chem Chem Phys 8(18):2153–2162
105. Batista ER, Xantheas SS, Jonsson H (1999) Multipole moments of water molecules in clusters and ice Ih. J Chem Phys 111(13):6011–6015